GRADUATE AERONAUTICAL LABORATORIES

CALIFORNIA INSTITUTE OF TECHNOLOGY

Whole-Field Measurements of Turbulent Flows for the Study of Aero-Optical Effects

D. C. Fourguette, P. E. Dimotakis and W. K. Ching

GALCIT Report FM96-8

7 October 1996

Firestone Flight Sciences Laboratory

Guggenheim Aeronautical Laboratory

Karman Laboratory of Fluid Mechanics and Jet Propulsion

Pasadena

Index-of-refraction imaging and aero-optics effects in a turbulent jet

D.C. Fourguette, P.E. Dimotakis, and W.K. Ching
Graduate Aeronautics Laboratories
California Institute of Technology
Pasadena, California 91125

Abstract

Planar laser-Rayleigh scattering has been employed to simultaneously image the index-of-refraction field of a turbulent jet of ethylene into nitrogen and the optical degradation of a laser sheet caused by this turbulent-flow field. The optical degradation occurs in the turbulent-jet region and manifests itself as phase-front tilts that result in a measurable spatial amplitude modulation (streaks) in the emerging pulsed-laser sheet. The experiments were conducted at elevated pressure, increasing the index-of-refraction gradients and improving the signal-to-noise ratio over measurements conducted at atmospheric pressure. The high index-of-refraction gradients in these experiments placed the optical far field within the field of view and allowed us to capture caustic formation in the distorted emerging laser sheet, simulating the aero-optics effects expected at large distances from the smaller index-of-refraction fluctuations one would more typically encounter.

7 October 1996

1. Introduction

Optical beams propagating through the atmosphere are subject to several degradation mechanisms arising from the index-of-refraction fluctuations along the path,[1] as well as blooming and self-focusing in the case of high-power lasers. For low-power lasers, the degradation can be described in terms of refraction deflections, or phase-front tilts, and loss of coherence. Long-range imaging through the atmosphere is subject to the same effects. Near-field phase-front tilts can produce focusing and defocusing in the optical far field, including the formation of caustics.[2,3]

Although optical aberrations sustained by a light beam propagating through an optically-nonuniform medium are routinely used for flow visualization purposes, *e.g.*, schlieren and shadowgraphy techniques, such aberrations are detrimental to applications such as astronomical and other imaging, as well as laser focusing through the turbulent atmosphere. Aero-optics effects produced by localized turbulence have been addressed by several investigators, *e.g.*, Refs. 4, 5, and 6. More recently, the small-aperture beam technique has helped elucidate the nature of optical aberrations caused by turbulent flow structures.[7–10] This technique evaluates the optical phase distortion by measuring optical-beam jitter and its relation to optical path differences.

A direct relation between optical distortion and identifiable features in the flow was established by Wissler and Roshko, who quantified the effects of spanwise and streamwise structures on the refraction of a small-diameter, collimated laser beam propagating through a turbulent shear layer.[11] In particular, Wissler & Roshko found that the optical aberrations were closely related to the large-scale structures in the flow, with best optical transmission occurring through the pre-transition region in the shear layer and worst in the transition region. These results were confirmed by Chew & Christiansen,[12] who used an optical beam with a diameter larger than the large-scale structure extent in the flow investigated.

The experiments presented here address both the mechanisms of optical distortion by a turbulent medium and the resulting distortion in the far optical field. The technique investigates the optical degradation mechanisms of a light sheet by a turbulent index-of-refraction field in a spatially- and time-resolved fashion using laser-Rayleigh scattering. The index-of-refraction distribution of a gas jet of ethylene (C_2H_4) into nitrogen (N_2) and the resulting optical degradation of the probe volume was measured using planar laser-Rayleigh light scattering. These two gases are density-matched so that the resulting turbulent flow is not subject to buoyancy

forces. As the light sheet propagates through the index-of-refraction field, light rays are refracted by index-of-refraction gradients and emerge from the turbulent flow-field with different in-plane, phase-front turning angles $\delta\theta$ proportional to the local transverse index-of-refraction gradient encountered along the path,[13]

$$\delta\theta = \int_0^L \frac{1}{n} (\nabla n)_\perp \, \mathrm{d}s \ . \tag{1}$$

In these experiments, the depth of field of the collecting optics is large enough to render the imaging insensitive to out-of-plane deflection of the probe beam (sheet). As a consequence, the data only register the in-plane distortions, $\delta\theta$, for which we have recorded the complete, in-plane index-of-refraction field of the turbulent jet, subject only to SNR limitations, *i.e.*,

$$\delta\theta \simeq \int_0^L \frac{1}{n} \frac{\partial n}{\partial y} \mathrm{d}x \ , \tag{2}$$

where y denotes the direction locally transverse to the x-propagation direction of the laser sheet. For the small total turning angles in this experiment, these directions may be regarded as constant, to a good approximation.

The experiments were carried out at elevated pressures to increase the signal and index-of-refraction gradients. The enhanced index-of-refraction gradients increase the optical turning angles, $\delta\theta$, decreasing the distance required for significant amplitude distortions to accumulate. In addition to causing larger optical distortions, the elevated pressure increases the number density of scatterers in the illuminated volume and, as a consequence, the signal-to-noise ratio of the measurements.

2. Experimental set-up

The experiment was conducted in the GALCIT High Pressure Reacting Vessel (HPRV).[14,15] Briefly, this vessel is capable of handling pressures in the range of $0.1\,\mathrm{atm} \leq p \leq 15\,\mathrm{atm}$. Its internal capacity is $1.43\,\mathrm{m}^3$ with an internal diameter of $1.07\,\mathrm{m}$.

The HPRV is equipped with several flow-management ports and 3 optical ports, consisting of (Pressure-Sight) polished-glass windows, 5 cm thick and 25 cm in diameter. The jet-nozzle exit is 1 cm in diameter and directed upward inside the tank. A choked-flow system ensures that the nozzle-fluid delivery is independent of the ambient tank pressure.

The schematics of the optical diagnostics system are depicted in Fig. 1.

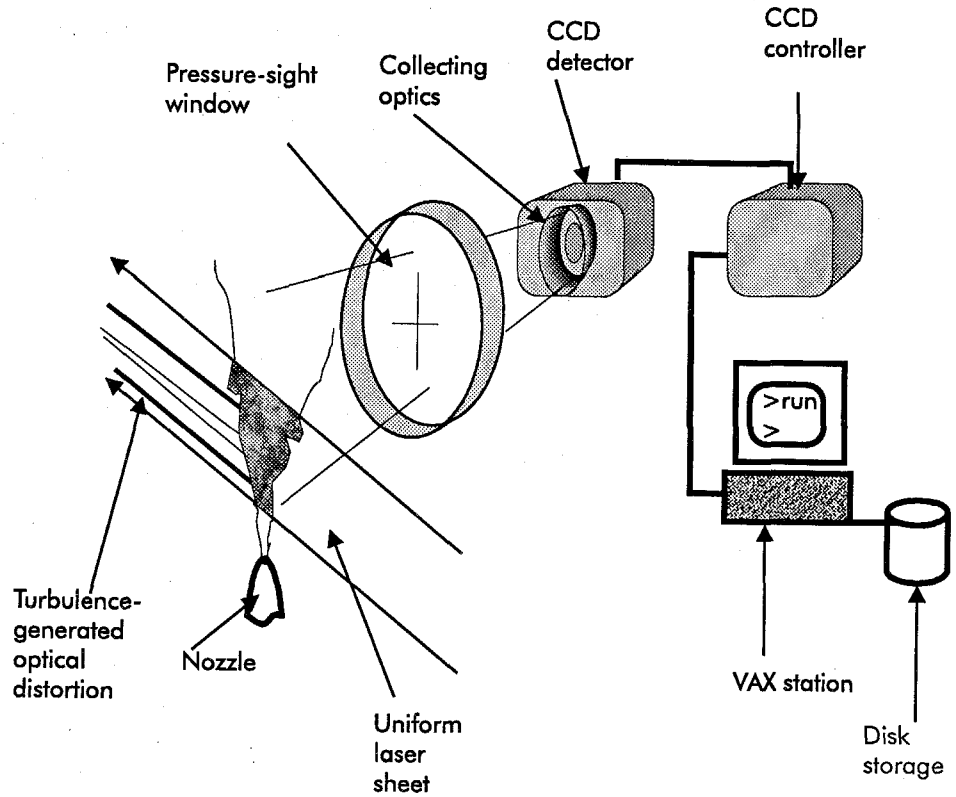

FIG. 1 Experimental set-up.

The beam of a frequency-doubled ($\lambda = 532\,\mathrm{nm}$), pulsed ($\tau \simeq 10\,\mathrm{ns}$) Nd:YAG laser was shaped into a sheet, passed through one of the optical ports, and included the jet centerline. The laser sheet was subsequently trapped into a beam-dump mounted inside the vessel to minimize spurious scattering and reflections. The Rayleigh-scattered light was collected at right angles outside the pressure vessel through a second optical port and imaged with a camera lens (85 mm focal length and f#1.9) onto a liquid-nitrogen-cooled, 1024^2-pixel, CCD array.

3. Experimental technique

The index-of-refraction of a gas, $n \simeq 1$, depends on the pressure. To leading order, we have,

$$n = 1 + \beta \frac{p}{p_0} . \tag{3}$$

In this expression, p is the ambient pressure, p_0 is a reference pressure, and β is the species-specific Dale-Gladstone constant. In the case of a gas mixture, the resulting index-of-refraction is the sum of the mole-fraction-weighted refraction indices, *i.e.*,

$$n_{\text{mix}} = \sum_i X_i n_i , \tag{4}$$

where X_i and n_i are the mole fraction and the index of refraction of the i^{th} gas species, respectively. Substituting Eq. 4 into Eq. 3 and for a binary gas mixture, the resulting index-of-refraction field becomes,

$$\begin{aligned} n_{\text{mix}} &= 1 + \frac{p}{p_0} \left[X\beta_2 + (1 - X)\beta_1 \right] \\ &= 1 + \frac{p}{p_0} \left[X(\beta_2 - \beta_1) + \beta_1 \right] , \end{aligned} \tag{5}$$

where X is the mole-fraction of one of the two gases, say, the jet-fluid gas. The index-of-refraction gradient in the y direction, then becomes,

$$\frac{\partial n}{\partial y} \simeq \frac{p}{p_0} (\beta_2 - \beta_1) \frac{\partial X(x,y)}{\partial y} . \tag{6}$$

Spatial derivatives of the pressure field have been ignored in this expression, as appropriate for the low Mach-number flow in these experiments and the dominant contribution of the gradients of local composition. Consequently, in this environment, index-of-refraction gradients are proportional to the (absolute ambient) pressure, p, and the local mole-fraction concentration (scalar-field) gradients. Elevated pressures also permit high Reynolds numbers and fully-developed turbulent flow to be obtained at moderate flow velocities, increasing the duration of quasi-steady flow in the confined enclosure (HPRV) in which the experiments were conducted.

Ethylene was chosen as the jet-fluid and nitrogen as the ambient fluid. Ethylene and nitrogen represent an ideal gas-pair because the difference in their index-of-refraction guarantees significant index-of-refraction gradients while being density-matched (same molecular mass).[16] Effects of buoyancy are thus obviated. For an C_2H_4 jet gas, $\beta_2 = 0.721 \times 10^{-3}$, while for the N_2 ambient gas, $\beta_1 = 0.300 \times 10^{-3}$.

Two-dimensional images of the index-of-refraction field were recorded using planar, laser-Rayleigh scattering. The Rayleigh-scattered intensity I_{sc} imaged on the CCD pixel area from a gas mixture is equal to

$$I_{sc}(x,y) = \Phi_0(x,y)\, N_s \frac{d\sigma_{mix}(x,y)}{d\Omega} \Delta\Omega\, A_{pixel}\, \eta_{opt}(x,y)\,, \tag{7}$$

where $\Phi_0(x,y)$ is the local fluence of the laser sheet at the imaged location (sheet intensity per unit transverse length), N_s is the number of scatterers in the probe volume, $\partial\sigma_{mix}(x,y)/\partial\Omega$ is the local differential Rayleigh-scattering cross-section of the illuminated gas mixture, $\Delta\Omega$ is the solid angle of the collecting optics, A_{pixel} is the relayed area of the corresponding CCD pixel (as relayed by the collecting optics on the laser sheet), and η_{opt} is the collecting optics efficiency.

At right angles, the differential scattering cross-section, $(\partial\sigma_{mix}/\partial\Omega)_{90°}$, depends on the wavelength of the incident light, λ, on the index of refraction of the gas, n, and on the number of scatterers, N_s, present in the illuminated volume. In particular, at right angles, we have,

$$\left(\frac{\partial\sigma}{\partial\Omega}\right)_{90°} = \frac{\pi^2}{\lambda^4}\left(\frac{n^2-1}{N_s}\right)^2 . \tag{8}$$

For gases and for the range of pressures employed in these experiments, the ratio $(n^2-1)/N_s$ is independent of the density, to a first approximation,[13] *i.e.*, the Rayleigh-scattering cross-section is independent of the pressure.

From these relations and for indeces of refraction near unity, the differential scattering cross-section of a gas mixture is the sum of the mole-fraction-weighted cross-sections, *i.e.*,

$$\frac{\partial\sigma_{mix}}{\partial\Omega} = \sum_i X_i \frac{\partial\sigma_i}{\partial\Omega}\,, \tag{9}$$

where X_i and $\partial\sigma_i/\partial\Omega$ are the mole fraction and differential scattering cross-section of i^{th} species, respectively.

As can be seen from Eq. 7, I_{sc} can be increased by increasing the number of scatterers in the probe volume, *i.e.*, the ambient pressure. The number of counts/pixel, N_{cts}, output by the CCD detector is directly proportional to the light scattered, I_{sc} reaching each pixel, and, therefore N_{cts} is also proportional to the pressure.

In the photon shot-noise-limited regime, as was the case in these measurements, the signal-to-noise ratio has the limiting behavior,

$$\text{SNR} \propto \sqrt{N_{cts}} \;\Rightarrow\; \text{SNR} \propto \sqrt{p}\,. \tag{10}$$

In summary, both index-of-refraction gradients and the signal-to-noise ratio of the measurements can be increased by increasing the ambient pressure of the experiment.

4. Results

Two individual realizations are reproduced in Figs. 2 and 3.

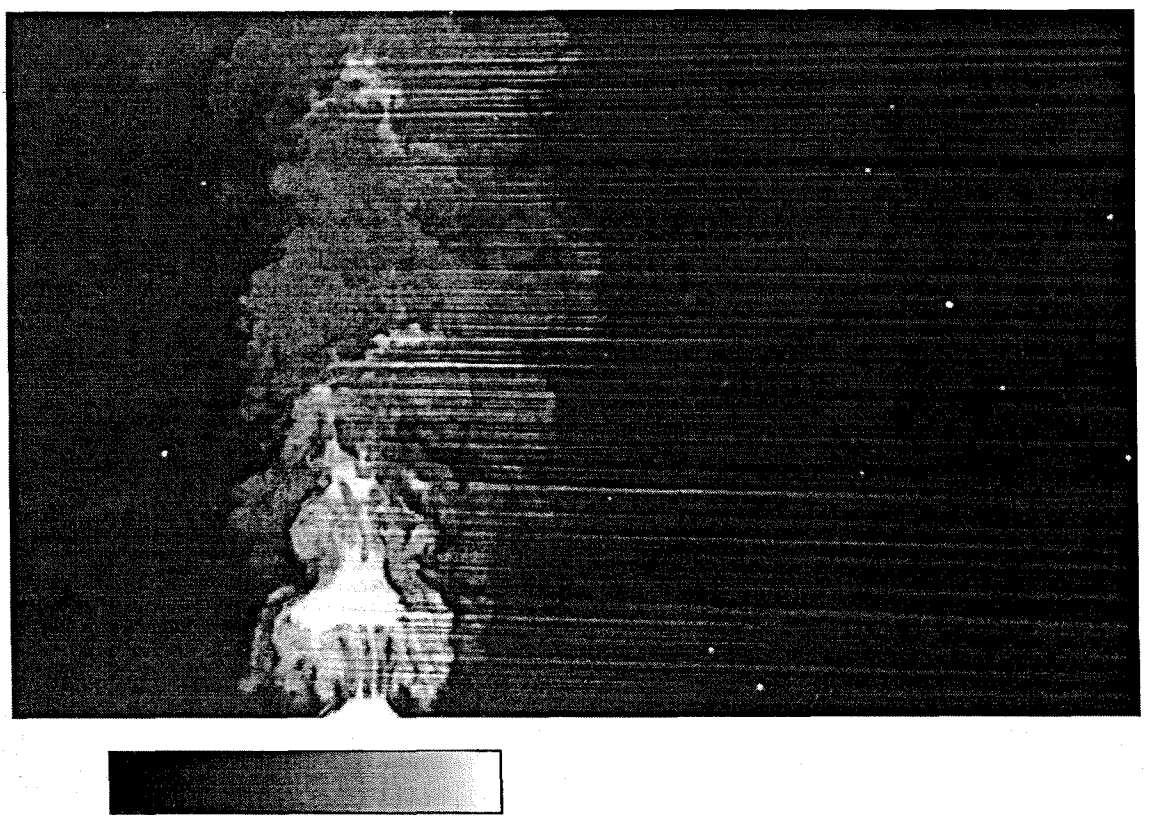

FIG. 2 Index-of-refraction field of and optical distortion by a turbulent jet, Re = 30,000.

FIG. 3 Index-of-refraction field of and optical distortion by a turbulent jet, $Re = 30{,}000$. See surface plot in Fig. 4 of intensity in circumscribed (300 × 300)-pixel region.

For these realizations, the jet Reynolds number, based on the nozzle-exit parameters, was $Re = 3 \times 10^4$, resulting in fully-developed turbulent flow.[17] While the scalar-fluctuation field possesses a continuous (spatial) spectrum, at this Reynolds number, the smallest-scale high-to-low (and vice-versa) transitions in the scalar (index of refraction) field are, approximately, 150 μm, or 300 μm for a high-to-low-to-high cycle (and vice-versa), in the imaged portion of the jet closest to the nozzle and, roughly, three times larger at the downstream end. These are estimated as the smallest diffusive scales expected for this flow, that are (for this $Sc \equiv \nu/\mathcal{D} \simeq 1$ flow), in turn, proportional to the computed local Kolmogorov scale.[16,18,19]

For all the experiments described here, the pressure in the vessel was maintained at $p = 10\,\text{atm}$. Photons incident on each pixel were collected from a probe

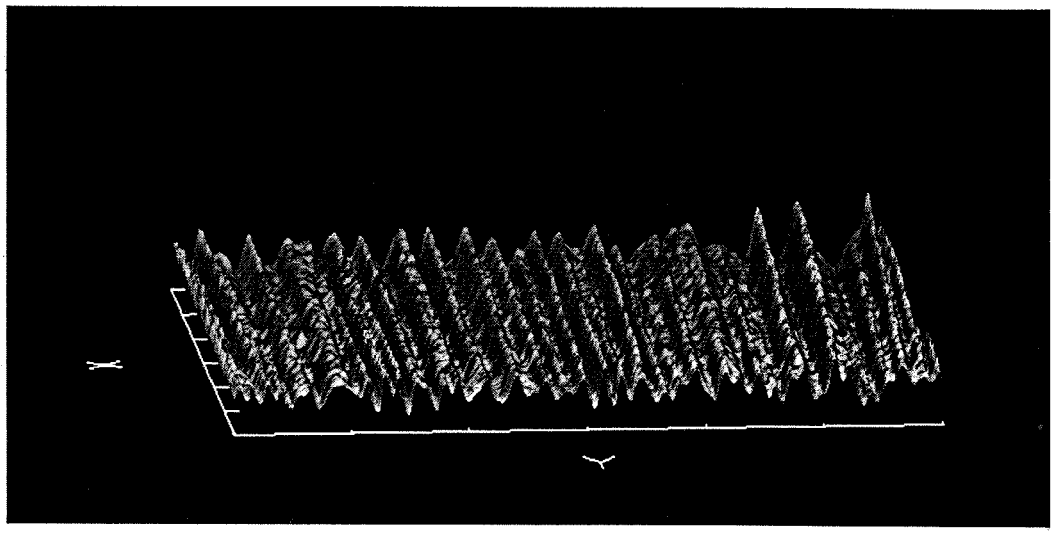

FIG. 4 Laser-fluence surface plot of resulting streaks (*cf.* Fig. 3).

volume,

$$V_{\text{probe}} \;=\; A_{\text{pixel}}\,\delta z \;=\; 140^2 \times 300\,\mu\text{m}^3 \tag{11}$$

(*cf.* Eq. 7 and associated discussion), where $\delta z = 300\,\mu$m is the estimated laser-sheet thickness. Figures 2 and 3 reproduce a (700×450)-pixel $(9.8 \times 6.3\,\text{cm}^2)$ portion of the data, capturing an imaged region of $3.3 \leq x/d \leq 9.3$ diameters downstream of the jet-nozzle exit. As a consequence, the laser-sheet thickness was comparable to (at $x/d \simeq 3.3$), or smaller than (for $x/d > 3.3$), the smallest estimated spatial scales within the imaged portion of the turbulent jet.

The raw image data, $I_{\text{raw}}(x,y)$, were corrected for background illumination and then normalized for any sheet-fluence, $\Phi(x,y)$ and collecting optics efficiency, $\eta_{\text{opt}}(x,y)$, non-uniformity over the field of view (*cf.* Eq. 7). The background-illumination field, $I_{\text{back}}(x,y)$, was obtained by averaging several images of the field of view, in the absence of scattered-light contributions from any test gas (evacuated vessel). Non-uniformities in the illuminating laser sheet and collecting optics were measured by averaging several images of a uniform index-of-refraction field, $I_{\text{field}}(x,y)$, derived from well-mixed ethylene and nitrogen, some time after each run. The background-corrected and normalized images were then calculated, on a pixel-by-pixel basis, as,

$$I_{\text{image}}(x,y) \;=\; \frac{I_{\text{raw}}(x,y) - I_{\text{back}}(x,y)}{I_{\text{field}}(x,y) - I_{\text{back}}(x,y)}\;.$$

The laser sheet propagates from left to right in both these images. The highest scattered-light intensity is depicted in white, while regions of low scattered-light intensity are dark. To the left of the jet flow-field, the light scattered off the pure-nitrogen ambient gas is uniform (after normalization). Light scattered off this pure-nitrogen region provides a reference for the maximum-scattered light intensity we can expect in the region of pure jet-fluid in the potential core, corresponding to pure ethylene, *i.e.*, $X = 1$. In the left portion of each image, where the right-propagating laser sheet has not accumulated significant fluence variations, the grey scale represents the mixture fraction of the local jet-fluid concentration, $X(x, y)$.

Horizontal streaks can be seen to originate from the turbulent flow-field region and are clearly registered in the reservoir-fluid region to the right of the turbulent-flow region. The fluid to the right of the jet-flow field is also the (pure N_2) ambient gas. As a consequence, the local Rayleigh-scattering cross section there is uniform and image intensity variations register local fluence variations of the optically-distorted laser sheet. The streak-like features are the optical aberrations caused by ray deflections (phase-front tilts) accumulated by propagation through the index-of-refraction gradients in the turbulent-jet flow field. Laser wave-fronts propagate through the flow-field and are refracted with a turning angle $\delta\theta$ proportional to the local transverse index-of-refraction gradient encountered along the path. In particular (*cf.* Eqs. 2, Eq. 6), we have,

$$\delta\theta \simeq \frac{p}{p_0}(\beta_2 - \beta_1) \int_0^L \frac{\partial X(x,y)}{\partial y}\,\mathrm{d}x \ . \tag{12}$$

The field of view in Fig. 3 extends to the right of the flow field to allow the evolution of the laser sheet to be registered.

Figure 4 is a surface plot of the image intensity in the region enclosed by the dotted, (300 × 300)-pixel square in Fig. 3. Crests indicate regions where the local laser fluence is high, *i.e.*, where rays are converging. Troughs indicate regions where laser fluence is low, *i.e.*, where rays are diverging. The rays (normal to the phase-fronts) emerge from the flow-field with different turning angles and propagate along straight paths, from then on, through the ambient (pure N_2) reservoir gas. Figure 4 includes examples of rays emerging with converging angles to form caustics, *i.e.*, when crests merge. One of these events, characterized by two rays merging and an increase in illumination intensity (fluence), can be seen on the right side of the fluence-surface plot.

The experiments described here simulate aero-optical effects that would be expected only at large distances from typically-encountered index-of-refraction fluctuation fields. In the small-angle deflection limit applicable here (Eq. 2), the distance, ℓ, where rays would cross and caustic formation may be expected will be scaled by the (reciprocal) of the index-of-refraction fluctuation amplitude (Eq. 13). Comparing two cases, a and b, with initial index-of-refraction differences, $\Delta n_{\rm a}$ and $\Delta n_{\rm b}$, in which all spatial scales are the same, we would have,

$$\frac{\ell_{\rm a}}{\ell_{\rm b}} = \frac{\Delta n_{\rm b}}{\Delta n_{\rm a}} \ . \tag{13}$$

By way of comparison, a slightly-heated turbulent air jet discharging into atmospheric-pressure air at the same Reynolds number ($Re = 3 \times 10^4$) as the one investigated here, would be characterized by the same distribution of spatial turbulent scales (both large and small). In the case of an atmospheric-pressure, heated jet with a temperature difference of, say, $\Delta T = 5\,{\rm K}$, we will have an index-of-refraction difference given by,

$$(\Delta n)_{\Delta T = 5\,{\rm K},\ {\rm air}} = \beta_1 \left(\frac{\rho_2 - \rho_1}{\rho_1} \right) = \beta_1 \left(\frac{\Delta T}{T_1} \right) \ , \tag{14a}$$

whereas, for the p-atmosphere ethylene-nitrogen jet investigated here (*cf.* Eqs. 3 and 6),

$$(\Delta n)_{C_2H_4,N_2} = \frac{p}{p_0} \left(\beta_2 - \beta_1 \right) \ . \tag{14b}$$

Consequently the ratio of initial index-of-refraction difference between the experiments described here and an atmospheric-pressure, $\Delta T = 5\,{\rm K}$ heated-air jet is estimated as (recall, $\beta_{C_2H_4}/\beta_{N_2} = \beta_2/\beta_1 = 0.721/0.300 \simeq 2.403$),

$$\frac{(\Delta n)_{C_2H_4,N_2}}{(\Delta n)_{\Delta T = 5\,{\rm K},\ {\rm air}}} \simeq \frac{p}{p_0} \left(\frac{\beta_2}{\beta_1} - 1 \right) \left(\frac{T_1}{\Delta T} \right) \simeq 842 \ , \tag{14c}$$

corresponding to a distance required to observe the same fluence-intensity variations (and caustics) of almost 850 times larger than with a $Re = 3 \times 10^4$, $\Delta T = 5\,{\rm K}$, heated-air jet.

5. Conclusions

The results presented here illustrate the degradation mechanisms sustained by a laser beam when propagating through non-uniformities in the index-of-refraction field caused by turbulence. The focusing (and defocusing) of the laser sheet indicates that turbulence-generated index-of-refraction gradients act as positive and negative refractive lenses. Index-of-refraction gradients and the attendant aero-optics effects can be enhanced by conducting such studies in an elevated-pressure environment. In the experiments reported here, the propagation distance by which significant amplitude distortions have accrued is sufficiently small to be within the field of view of a laboratory-scale experiment, simulating effects that would require much greater propagation paths in the atmosphere. The refraction angles of optical rays, as they emerge from the turbulent region, in these experiments, are sufficiently large to form caustics within the imaged field of view.

6. Acknowledgements

This work was sponsored by the Air Force Office of Scientific Research, under Grant No. F49620–94–1–0283. The US Government is authorized to reproduce and distribute reprints for Governmental purposes notwithstanding any copyright notation thereon.

References

[1] Tatarskii, V. I., *The effects of the turbulent atmosphere on wave propagation* (McGraw-Hill, New York, 1961).

[2] Kulkarny, V. A., and White, B. S., "Focusing of waves in turbulent inhomogeneous media," *Phys. Fluids* **25**(10), 1770–1784 (1982).

[3] Freid, D. L., and Vaughn, J. L., "Branch cuts in the phase function," *Appl. Optics* **31** (15), 2865–2882 (1992).

[4] Gilbert, K. G., and Otten, L. J., *Aero-Optical Phenomena* (*Progress in Astronautics and Aeronautics* **80**, , 1982).

[5] Sutton, G. W., "Aero-optical foundations and applications," *AIAA J.* **23**(10), 1525–1537 (1985).

[6] Klein, H. H., Malley, M. M., Sapp, O., Shough, D., Sutton, G. W., and Yu, J. H.-Y., "Experimental Measurements of the Optical Path Difference of a Four-Meter Dual Aerocurtain," in *Propagation of High-Energy Laser Beams through the Earth's Atmosphere*, SPIE Proceedings **1221** (1990).

[7] Malley, M. M., Sutton, G. W., and Kincheloe, N., "Beam-jitter measurements of turbulent aero-optical path differences," *Appl. Optics* **31**(22), 4440–4443 (1992).

[8] Jumper, E.J., and Hugo, R.J., "Optical phase distortion due to turbulent fluid density fields: Quantification using the small-aperture beam technique," *AIAA* 23rd *Plasma Dynamics and Lasers Conference*, Paper 92–3020 (1992).

[9] Hugo, R. J., and Jumper, E. J., "Experimental measurement of a time-varying path difference using the small-aperture beam technique," Proc. 1993 SPIE Int. Symp. on Optics, Imaging, and Instrumentation (June 1993, San Diego), SPIE #2005–13 (1993).

[10] Hugo, R.J., Jumper, E.J., Havener, G., and Stepanek, S.A., "Time-resolved, aero-optical measurements of a wavefront aberrated by a compressible free shear layer," *AIAA* 26th *Plasmadynamics and Lasers Conference*, Paper 95–1979 (1995).

[11] Wissler, J. B., and Roshko, A., "Transmission of Thin Light Beams Through Turbulent Mixing Layers," *AIAA* 30th *Aerospace Sciences Meeting*, AIAA–92–0658 (1992).

[12] Chew, L., and Christiansen, W., "Experimental investigation of transitional free shear layer optics," *AIAA J.* **31**(12), 2290–2295 (1993).

[13] Born, M., and Wolf, E., *Principles of Optics* (6th edition, Pergamon Press, Oxford, 1993).

[14] Gilbrech, R. J., *An Experimental Investigation of Chemically-Reacting, Gas-Phase Turbulent Jets*, Ph.D. thesis, California Institute of Technology (1991).

[15] Gilbrech, R. J., and Dimotakis, P. E., "Product Formation in Chemically-Reacting Turbulent Jets," *AIAA* 30th *Aerospace Sciences Meeting*, Paper 92–0581 (1992).

[16] Dowling, D. R., and Dimotakis, P. E., "Similarity of the concentration field of gas-phase turbulent jets," *J. Fluid Mech.* **218**, 109–141 (1990).

[17] Dimotakis, P. E., "Some issues on turbulent mixing and turbulence," GALCIT Report FM93–1a (1993).

[18] Miller, P. L., and Dimotakis, P. E., "Reynolds number dependence of scalar fluctuations in a high Schmidt number turbulent jet," *Phys. Fluids A* **3**, 1156–1163 (1991).

[19] Miller, P. L., and Dimotakis, P. E., "Measurements of scalar power spectra in high Schmidt number turbulent jets," *J. Fluid Mech.* **308**, 129–146 (1996).